Optic phonon bandwidth and lattice thermal conductivity: The case of Li_{2}X (X=O, S, Se, Te)

S. Mukhopadhyay, L. Lindsay, and D. S. Parker

Phys. Rev. B **93**, 224301 — Published 7 June 2016

DOI: 10.1103/PhysRevB.93.224301

Optic phonon bandwidth and lattice thermal conductivity: the case of Li_2X (X=O, S, Se, Te)

S. Mukhopadhyay, L. Lindsay* and D. S. Parker

Materials Science and Technology Division, Oak Ridge National Laboratory, Oak Ridge,

Tennessee 37831, USA

Optic phonon bandwidth and lattice thermal conductivity: the case of Li_2X (X=O, S, Se, Te)

S. Mukhopadhyay, L. Lindsay* and D. S. Parker

Materials Science and Technology Division, Oak Ridge National Laboratory, Oak Ridge, Tennessee 37831, USA

Abstract

We examine the lattice thermal conductivities (κ_l) of Li_2X (X=O, S, Se, Te) using a first-principles Peierls-Boltzmann transport methodology. We find low κ_l values ranging between 12 and 30 W/m-K despite light Li atoms, a large mass difference between constituent atoms and tightly bunched acoustic branches, all features that give 'high κ_l' in other materials including BeSe (630 W/m-K), BeTe (370 W/m-K) and cubic BAs (3170 W/m-K). Together these results suggest a missing "ingredient" in the basic guidelines commonly used to understand and predict κ_l. Unlike typical simple systems (*e.g.*, Si, GaAs, SiC), the dominant resistance to heat-carrying acoustic phonons in Li_2Se and Li_2Te comes from interactions of these modes with two optic phonons. These interactions require significant bandwidth and dispersion of the optic branches, both present in Li_2X materials. These considerations are important for the discovery and design of new materials for thermal management applications, and give a more comprehensive understanding of thermal transport in crystalline solids.

PACS: 66.70.-f, 63.20.Kr, 71.15.-m, 72.15.Jf, 44.10.+i, 63.20dk

I. INTRODUCTION

Exciting recent advances, including the advent of *predictive first principles* calculations of lattice thermal conductivity [1-5] (κ_l) and microscopic experimental probes of κ_l accumulation [6-8], are deepening our physical understanding of thermal transport in solids. The design of future materials and technologies to address critical needs ranging from waste heat recovery (low κ_l thermoelectrics) [9] to heat management in nano- and micro-electronics (*e.g.*, high κ_l heat sinks and thermal interface materials) [10], hinges on this understanding. In terms of "high κ_l" materials, diamond [11-13] is the long-standing champion for bulk materials, with graphene [14,15] more recently reinforcing the view that carbon-based materials are the best heat conductors. Excellent heat transport properties of these systems have been attributed to (I) simple structure, (II) light atomic mass, (III) strong covalent bonding (high Debye temperature - θ_D) and (IV) low anharmonicity [16,17]. These guidelines have helped researchers understand and predict, albeit qualitatively, intrinsic heat transport in a variety of systems.

However, more recent first principles predictions of κ_l in GaN [18] and BAs [19] have transformed this simple picture. New guidelines have emerged, based on the microscopic phase space for scatterings of phonons. In particular, phase space for intrinsic three-phonon interactions (arising from crystal anharmonicity, lowest order in perturbation theory) is limited by (V) a frequency gap between heat-carrying acoustic (*a*) phonons and high frequency optic (*o*) phonons (*a*-*o* gap) and (VI) bunching of the acoustic branches. The *a*-*o* gap is often determined by mass mismatch between constituent atoms and governs the interaction of two acoustic phonons with an optic phonon, *aao* scattering. Bunching of acoustic modes occurs in materials with one of the constituent atoms from row II of the periodic table (empirically determined) [18-21] which governs interactions of three acoustic phonons, *aaa* scattering. We note that phonon

scattering from naturally occurring isotope variation can also play a role in limiting κ_l, though may not be considered an intrinsic material property as isotope concentrations can be manipulated.

In this article, we propose another intrinsic condition that can be equally important for determining κ_l: *optic phonon bandwidth* (overall optic frequency range) *and dispersion*. In this context, we examine thermal transport in anti-fluorite Li_2X (X=O, S, Se, Te) materials. In particular, we discuss phonon features that Li_2Se and Li_2Te have in common with high conductivity materials BAs and GaN (calculated κ_l values of 3170 [19] and 400 [18] W/m-K, respectively), namely large *a-o* gaps and very bunched acoustic branches. Despite sharing these features, which were shown to give high κ_l in these systems, Li_2Se and Li_2Te have poor conductivities with calculated room temperature values of 17.7 and 14.7 W/m-K, respectively. Therefore, the six conditions described initially are not sufficient to ensure high κ_l. The optic bandwidth and dispersion determine the phase space for *aoo* scattering for which an acoustic phonon must have a frequency less than or equal to the optic bandwidth in order to conserve energy. Thus, for prototypical simple cubic semiconductors (*e.g.*, Si, Ge, GaAs) with small optic bandwidths and appreciably flat optic branches, *aoo* processes can only scatter very low frequency acoustic phonons, and do not dictate the overall κ_l behavior in such materials. By contrast, all four Li_2X materials display substantial optic bandwidth and dispersion, greatly expanding the phase space available for *aoo* scattering, yielding a large reduction in κ_l.

We briefly note that Li_2O is a candidate tritium breeding material for fusion reactors [22,23]. Li_2Te is of interest in alternative solid state battery systems[24], and Li_2Se/Te alloys have been proposed for neutron scintillator materials[25].

II. COMPUTATIONAL DETAILS

We employed density functional theory (DFT) [26,27] within both its local density approximation (LDA) and its generalized gradient approximation (GGA) for energy minimization and interatomic force constant (IFC[28]) calculations. We used norm conserving pseudopotentials for each atom (Li-pz-n-vbc, O-pz-mt, S-pz-bhs, Se-pz-bhs and Te-pz-bhs for LDA; Li-pbe-mt, O-pbe-mt, S-pbe-mt and Se-pbe-mt for GGA) [29] with a plane wave cutoff energy of 100 Ry and a convergence threshold of 10^{-14} Ry (difference of energies between two consecutive SCF cycles). We used a 16×16×16 Monkhorst-Pack grid for electronic structure calculations. The LDA calculated equilibrium lattice parameters (a) are ~3% underestimated for each case (a_{Li_2O}=4.46 Å, a_{Li_2S}=5.53 Å, a_{Li_2Se}=5.83 Å and a_{Li_2Te}=6.33Å) relative to their corresponding experimental values (a_{Li_2O}=4.62 Å [30], a_{Li_2S}=5.71 Å[31], a_{Li_2Se}=6.00 Å [32] and a_{Li_2Te}=6.51 Å [33]). This is consistent with the usual shortcomings of LDA which typically over-binds systems [34]. Interestingly, GGA calculations give lattice constants (a_{Li_2O}=4.52 Å, a_{Li_2S}=5.64 Å, a_{Li_2Se}=5.96 Å and a_{Li_2Te}=6.52 Å) that are in better agreement, though smaller than experiment in most cases as GGA calculations typically under-bind the atoms. The harmonic IFCs were calculated using density functional perturbation theory with an 8×8×8 *q-mesh* as implemented in Quantum Espresso [35]. We used a supercell approach to calculate third order anharmonic IFCs based on DFT. We considered Γ-point-only calculations on supercells with 324 atoms, and included interactions out to the sixth nearest neighbors of the unit cell atoms with an energy convergence threshold of 10^{-10} Ry. Finally, three-phonon scattering rates, $1/\tau_{\vec{q}j}$, [36] were calculated and the lattice thermal conductivity $\kappa_l = \sum_{\vec{q}j} C_{\vec{q}j} v_{\vec{q}j}^2 \tau_{\vec{q}j} / V$ was determined from a fully iterative solution of the Peierls-Boltzmann equation based on the harmonic and anharmonic IFCs. Here, $C_{\vec{q}j} = k_B n_{\vec{q}j}^0 (n_{\vec{q}j}^0 + 1)(\hbar\omega_{\vec{q}j} / k_B T)^2$ is the specific heat per phonon mode, $v_{\vec{q}j}$ is the group

velocity, V is the crystal volume, k_B is the Boltzmann constant, and $\vec{q}$ and j designate the wave vector and branch index of a phonon with frequency $\omega_{\vec{q}j}$. $n^0_{\vec{q}j}$ is the Bose distribution. Further details of the calculation can be found elsewhere [36-38] .

Each scattering process must conserve crystal momentum and energy, $\vec{q} \pm \vec{q}' = \vec{q}'' + \vec{G}$ and $\omega_{\vec{q}j} \pm \omega_{\vec{q}'j'} = \omega_{\vec{q}''j''}$, where $\vec{G}$ is a reciprocal lattice vector that is zero for Normal processes and non-zero for Umklapp processes. These conditions restrict the phase space for *aaa*, *aao*, *aoo* and *ooo* scattering. We note that there are nine phonon branches in the Li_2X systems with three acoustic and six optic modes. We characterize the type and amount of scattering for each phonon mode by calculating the mode-dependent phonon phase space:

$$P_{\vec{q}jj'j''} = \sum_{\vec{q}'\vec{q}''} \{\delta(\vec{q} + \vec{q}' - [\vec{q}'' + \vec{G}])\delta(\omega_{\vec{q}j} + \omega_{q'j'} - \omega_{\vec{q}''j''}) + \frac{1}{2}\delta(\vec{q} - \vec{q}' - [\vec{q}'' + \vec{G}])\delta(\omega_{\vec{q}j} - \omega_{q'j'} - \omega_{\vec{q}''j''})\} \qquad (1)$$

Please note that we break this phase space term and the scattering rates into different types (*aaa*, *aao*, *aoo* and *ooo*) based on the branch index j, j' and j'' of phonons involved in the scattering process.

In analyzing the thermal transport properties of these systems we also calculate Debye temperatures, θ_D, and average Grüneisen parameters, $\bar{\gamma}$, given by:

$$\theta_D = \frac{\hbar}{k_B} v_D \sqrt[3]{\frac{6\pi^2 N_0}{V}} \qquad (2)$$

$$\bar{\gamma} = \sum_{\vec{q}j} C_{\vec{q}j} \left|\gamma_{\vec{q}j}\right| \Big/ \sum_{\vec{q}j} C_{\vec{q}j} \qquad (3)$$

$\hbar$ is the reduced Planck constant, N_0 is the number of atoms, and v_D is the Debye velocity given by:

$$v_D^{-3} = \frac{1}{3} v_{LA}^{-3} + \frac{2}{3} v_{TA}^{-3} \tag{4}$$

with v_{LA} and v_{TA} being the longitudinal and transverse sound velocities. The sound velocities were determined from the zone-center phonon dispersions of each material in the $\Gamma \to X$ high symmetry direction. We note that group velocities may vary along different crystal directions, and so too the calculated Debye temperature. However, the variation in the calculated Debye temperature along different symmetry axes fall within 10% of the average for all Li_2X systems. $\gamma_{\vec{q}j}$ is the mode Grüniesen parameter given by [39]:

$$\gamma_{\vec{q}j} = -\frac{1}{6\omega_{\vec{q}j}^2} \sum_{\kappa} \sum_{l'\kappa'} \sum_{l''\kappa''} \sum_{\alpha\beta\gamma} \Phi_{\alpha\beta\gamma}(0\kappa, l'\kappa', l''\kappa'') \frac{e_{\alpha\kappa}^{\vec{q}j*} e_{\beta\kappa'}^{\vec{q}j}}{\sqrt{\overline{m}_\kappa \overline{m}_{\kappa'}}} e^{i\vec{q}\cdot\vec{R}_{l'}} r_{l''\kappa''\gamma} \tag{5}$$

T is temperature, $r_{l\kappa\alpha}$ is the α^{th} component of the vector locating the κ^{th} atom in the l^{th} unit cell, $e_{\alpha\kappa}^{\vec{q}j}$ is the eigenvector for this atom and component, and $\overline{m}_\kappa$ is the isotope averaged mass for this atom. $\vec{R}_l$ is a lattice vector and $\Phi_{\alpha\beta\gamma}(0\kappa, l'\kappa', l''\kappa'')$ are the third order anharmonic IFCs[28].

III. RESULTS AND DISCUSSION

As discussed in the previous section, the GGA calculations give better agreement with measured lattice constants of these systems. This is reflected in the comparison of phonon dispersions of Li_2O and Li_2S with their corresponding measured dispersions (see Appendix A). Regardless, we performed LDA calculations for comparison as these were employed in numerous previous calculations on other systems and give an upper bound to predicted κ_l values.

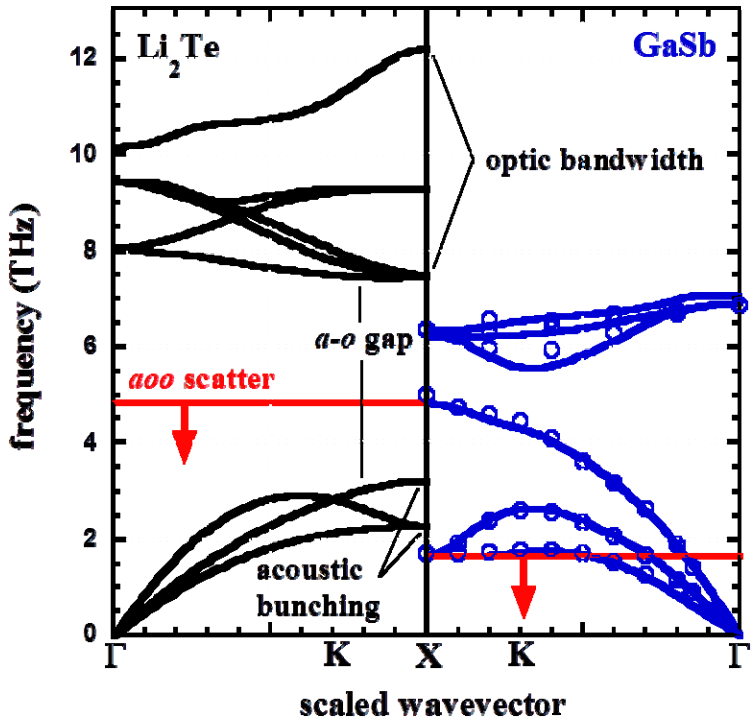

Figure 1: Calculated phonon dispersions for Li_2Te (black curves) and GaSb (blue curves) in the Γ→K→X direction. Blue circles give measured data for GaSb [40] . The red lines correspond to calculated optic bandwidth for each material. Given conservation of energy, only acoustic phonons below these lines can participate in aoo scattering.

Figure 1 shows the calculated phonon dispersion of Li_2Te in the Γ→K→X direction compared to a typical cubic compound material, GaSb (see Appendix A for dispersions of other Li_2X systems). We compare dispersions of these systems to highlight important vibrational features that govern κ_l. In Li_2Te, the large mass difference between light Li atoms that govern optic frequencies and heavy Te atoms that govern acoustic frequencies results in a large *a-o* gap that disallows all *aao* scatterings as they cannot conserve energy. This feature was important for understanding high conductivities of BAs [19] and GaN [18]. Like these high κ_l systems, Li_2Te also satisfies Condition (VI) above, namely the acoustic branches are very tightly bunched (see Fig. 1 and Table I). This results in a severely reduced *aaa* scattering phase space and typically gives rise to higher κ_l in systems without *aao* scattering. Surprisingly, however, calculated room

Table I: Dispersion features that determine κ_l: (II) and (III) bonding and average mass (M_{avg}) – Debye temperature (θ_D); (V) *a-o* gap – $(\omega^o_{\min} - \omega^a_{\max})/\omega^a_{\max}$; (VI) acoustic branch bunching – $(\omega^{LA}_X - \omega^{TA}_X)/\omega^{LA}_X$; (VII) optic bandwidth – $(\omega^o_{\max} - \omega^o_{\min})/\omega^a_{\max}$. Here ω^{LA}_X and ω^{TA}_X are calculated longitudinal and transverse acoustic frequencies at the X point, respectively, and $\omega^o_{\max}$, $\omega^o_{\min}$ and $\omega^a_{\max}$ are calculated maximum optic, minimum optic and maximum acoustic frequencies, respectively. Note: (i) larger *a-o* gap gives **less** *aao* scattering (>1 gives **no** *aao* scattering); (ii) larger acoustic bunching gives **more** *aaa* scattering; (iii) larger optic bandwidth gives **more** *aoo* scattering. Calculated room temperature κ_l for natural and isotopically pure materials using LDA [GGA] are also given. GGA gives lower values but similar trends. All other calculations were done using LDA.

Condition	Li_2O	Li_2S	Li_2Se	Li_2Te	BeS	BeSe	BeTe	BAs	Si
(II and **III)** θ_D (K)	834	538	371	265	759	496	361	716	707
(V) scaled *a-o* gap	□	0.01	0.64	1.26	0.39	1.08	1.68	0.93	□
(VI) scaled acoustic bunching	0.39	0.22	0.23	0.29	0.38	0.36	0.39	0.40	0.67
(VII) scaled optic bandwidth	**1.04**	**0.94**	**1.41**	**1.49**	**0.40**	**0.69**	**0.72**	**0.35**	**0.40**
κ_l pure (W/m-K) LDA [GGA]	31.2 [21.1]	18.9 [13.24]	17.7 [10.83]	14.7 [10.14]	195	633	371	3170	155
κ_l natural (W/m-K) LDA [GGA]	29.26 [20.12]	16.99 [12.13]	14.88 [9.47]	12.48 [7.01]	176	115	102	2240	145

temperature κ_l for isotopically pure Li_2Se (17.7 W/m-K) and Li_2Te (14.7 W/m-K) are substantially lower than that of BAs (3170 W/m-K) [19] and GaN (400 W/m-K) [18]. Further, κ_l in these systems are more than an order of magnitude lower that their Beryllium chalcogenide counterparts, BeSe (633 W/m-K) and BeTe (371 W/m-K) [21], despite having similar structure, masses and more tightly bunched acoustic branches (see Table I). The objective of this study is to understand the origin of low κ_l of Li_2X systems, and to expand the simple guidelines that direct our understanding of κ_l and our search for alternative high conductivity materials.

Figure 2 gives calculated κ_l for Li_2X materials as a function of temperature for systems with naturally occurring isotope concentrations. At higher temperature each system demonstrates the typical T^{-1} dependence of κ_l with increasing temperature, characteristic of intrinsic three-phonon scattering. The only measured κ_l in the literature for Li_2X systems is for Li_2O for porous samples[22,23] from sintered material with significant impurities[23]. Black circles are data from Ref. [23] with 93.5% of the theoretical density. The LDA values for κ_l of Li_2O are ~2 times higher than Ref.[23], while GGA values give better agreement, though still somewhat larger than experiment. The extrinsic scattering created by grain boundaries and impurities in these sintered, porous systems may cause the measured κ_l values to fall significantly below the calculated single crystal values, as we observe. The agreement between calculated and measured κ_l becomes progressively better as temperature increases. This is precisely the effect one would expect as extrinsic scattering is largely T-independent, while phonon-phonon scattering *increases* with temperature. The differences between LDA and GGA κ_l calculations can largely be attributed to differences in the bonding and subsequent lattice constants. GGA gives larger lattice constants, which gives lower optic phonon frequencies. These optic modes then couple more strongly with the acoustic modes, thus reducing κ_l when compared to LDA calculations. We note also that a recent model calculation found agreement with this Li_2O κ_l data with parameters adjusted to fit other measured properties[41].

As shown by black circles in the inset to Fig. 2, calculated room temperature κ_l of Li_2X materials monotonically decreases with decreasing Debye temperature, θ_D, (indicative of decreasing acoustic velocities) in going from X=O to S to Se to Te. This κ_l behavior is similar to that demonstrated by elemental materials diamond, Si and Ge, [20] and can be understood in terms of an increase in average mass, M_{avg}, suppressing θ_D and acoustic velocities. However,

Li_2X are compound materials for which increasing M_{avg} is accompanied by an increasing mass difference between constituent atoms, which results in an increased *a-o* gap and reduced *aao* scattering [42] for Li_2Se and Li_2Te systems. Thus monotonically decreasing κ_l behavior for the chalcogen varying from O to S to Se to Te is surprising, especially when contrasted with the behavior demonstrated by Boron-based [20] and Beryllium-based compounds (inset to Fig. 2) [21].

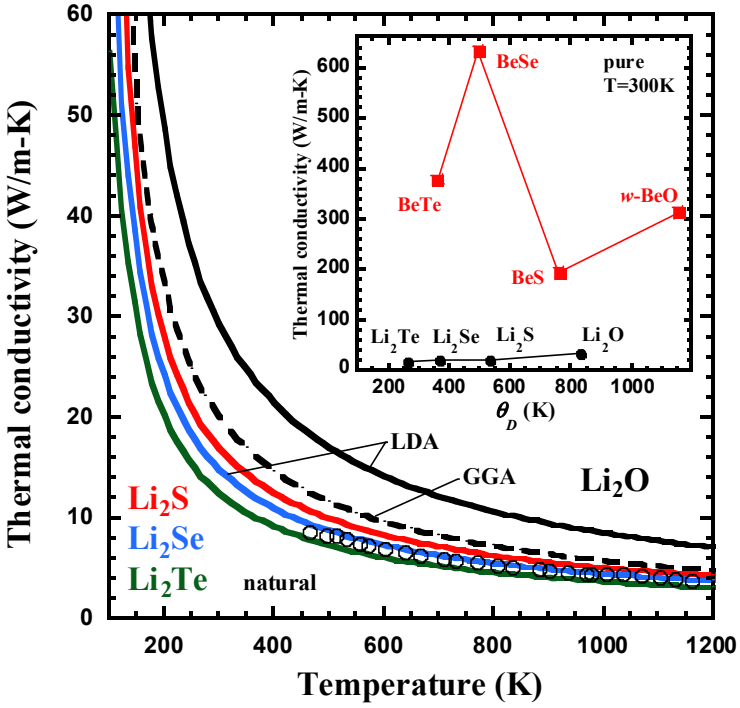

Figure 2: Calculated κ_l with naturally occurring isotope concentrations versus temperature for Li_2O (black; solid-LDA, dashed-GGA), Li_2S (red), Li_2Se (blue), Li_2Te (green). Black circles give measured Li_2O κ_l from Ref.[23] for a scintered, porous sample. The inset gives calculated pure κ_l (at 300K) versus Debye temperature, θ_D, for Li_2X (black) and BeX (red). The lines are guides for the eyes. GGA calculations for Li_2S, Li_2Se and Li_2Te (not shown) give smaller values than the LDA calculations (~30-40% lower).

This gives a clue that *aao* scattering processes are not responsible for the low conductivities of the Li_2X systems. We also note that mass ratio is not the only governing factor in determining

the *a-o* gap[43]. For example, rocksalt CdO has a mass ratio of 7, slightly larger than BAs, yet has almost no *a-o* gap due to the nature of atomic bonding and optic dispersion in that system [44].

To further investigate the origin of low κ_l in Li_2X, we focus on different three-phonon scattering channels and their correlation with features of the phonon dispersions. Figure 3 shows calculated scattering rates, $1/\tau_{\tilde{q}j}$ for acoustic modes of Li_2Te and BAs, systems with very different predicted κ_l values.

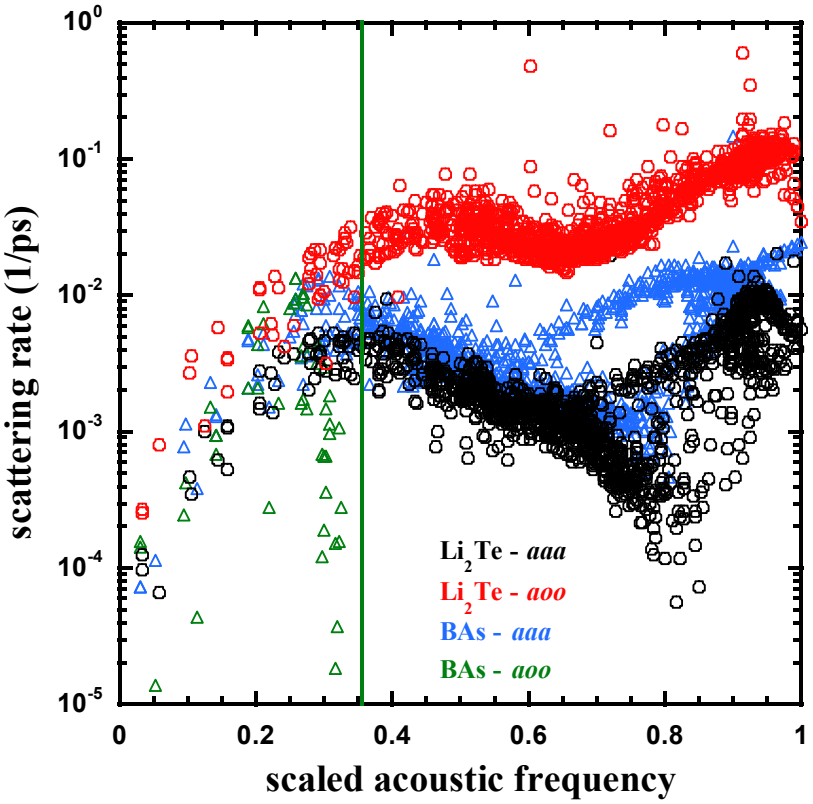

Figure 3: Calculated acoustic phonon scattering rates versus scaled acoustic frequency for aaa processes in Li_2Te (black circles), aoo processes in Li_2Te (red circles), aaa processes in BAs (blue triangles) and aoo processes in BAs (green triangles). The frequencies are scaled by the maximum longitudinal acoustic frequency of each system. The horizontal green line shows the optic bandwidth for BAs above which no aoo processes can occur. Both systems lack aao scattering due to their large a-o gaps.

The corresponding calculated phase spaces are given by Fig. 4. Scattering rates for the other Li_2X systems can be found in Appendix B. Note that *aao* scattering and *ooo* scattering are not possible in either Li_2Te or BAs due to conservation of energy. Both systems have relatively weak *aaa* scattering due to acoustic phonon branches that are tightly bunched (see Fig. 1 for Li_2Te and Fig. 2 in Ref. [19] for BAs). This bunching severely reduces the possible phase space for *aaa* scattering, which coupled with no *aao* scattering was shown to give the predicted ultrahigh κ_l for BAs [19]. The six conditions for high κ_l described above are all met to some degree. Therefore, it is surprising that the κ_l values of Li_2Te (and the other Li_2X materials) are orders of magnitude lower than that of BAs. What is the origin of the low κ_l of Li_2X systems?

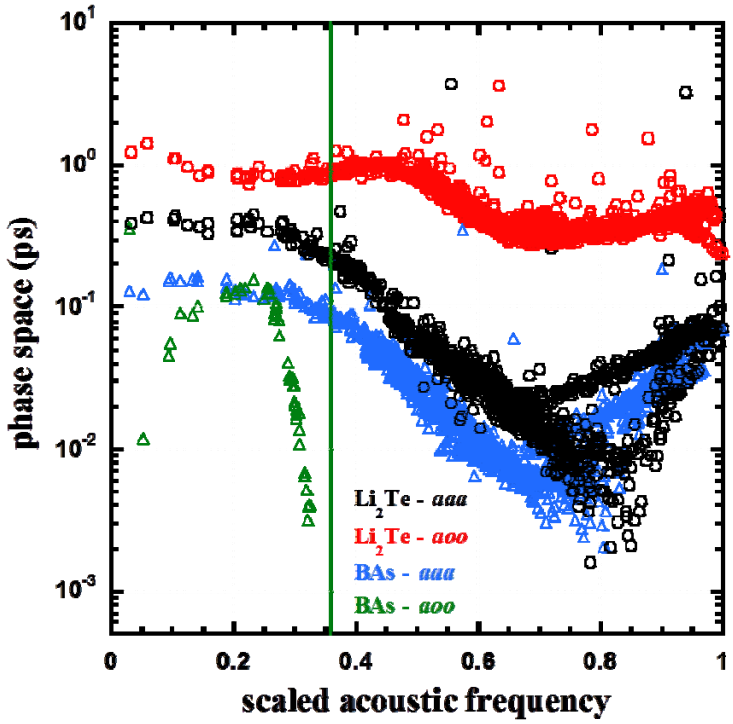

Figure 4: Calculated three-phonon scattering phase space (Eq. 1) versus scaled acoustic frequency for aaa processes in Li_2Te (black circles), aoo processes in Li_2Te (red circles), aaa processes in BAs (blue triangles) and aoo processes in BAs (green triangles). The frequencies are scaled by the maximum longitudinal acoustic (LA) frequency of each system. The vertical green line shows the calculated optic bandwidth for BAs above which no aoo processes can occur. Li_2Te and BAs have no aao scattering due to their large a-o gaps.

Despite large *a-o* gaps in Li_2Se and Li_2Te, optic phonons play an important role in scattering of heat-carrying acoustic phonons via *aoo* scattering channels. For typical fcc cubic semiconductors *aoo* scattering is negligible across much of the acoustic frequency spectrum (Fig. 1 for GaSb and Fig. 3 for BAs), however, for Li_2Te and other Li_2X systems this scattering is the dominant resistance to heat flow. In typical cubic semiconductors the bandwidth of optic phonons is relatively small compared to the bandwidth of acoustic phonons (calculated as the highest frequency acoustic mode). This is demonstrated by the red line in Fig. 1 for GaSb which represents a hard boundary for *aoo* scattering: acoustic modes with frequencies below find appreciable *aoo* scattering, acoustic modes above cannot conserve energy in an *aoo* process. This is reflected in the phase space (Fig. 4) and lack of *aoo* scattering for BAs in Fig. 3. In Li_2X materials, optic bandwidth is so large that all acoustic modes (nearly all in Li_2S) can scatter with two optic modes and conserve energy. This gives rise to very strong resistive *aoo* scattering, more than an order of magnitude larger than the corresponding *aaa* scattering rates for most of the acoustic spectrum in Li_2Te (Fig. 3). Since scattering rates are inversely proportional to mean free path (and κ_l), this explains the low κ_l in Li_2X systems when compared to other zinc blende cubic structures. Thus, we propose that a seventh condition be added to the common intrinsic guidelines used to estimate κ_l: (VII) *optic phonon bandwidth.* These guidelines may be applied to nanoscale systems (*e.g.*, graphene, MoS_2, nanotubes) as long as other important symmetry constraints are considered. We also note that *aoo* interactions are important for understanding optic phonon relaxation (*e.g.*, hot phonon effects in III-Nitrides)[42,45-47], for describing κ_l of carbon nanotubes [48,49] and for understanding low κ_l in IV-VI semiconductors [48,50-52].

Further, optic bandwidth alone is not sufficient to guarantee significant *aoo* scattering; dispersion of individual optic branches is also necessary. In order for the entire range of possible

acoustic modes to be involved in *aoo* scatterings there must be a range of energy differences between two optic phonons. To elucidate this, imagine a material with an optic bandwidth larger than the acoustic bandwidth, but with perfectly flat optic branches distinct in frequency. In this case, the frequency difference between two optic phonons is constant and larger than all acoustic frequencies, *i.e.*, no *aoo* scattering can occur. For most materials, however, transverse and longitudinal optic branches disperse through much of the optic bandwidth and often cross (see Fig. 1). Thus, examination of optic bandwidth is typically a good indicator of the strength of *aoo* scattering in a material.

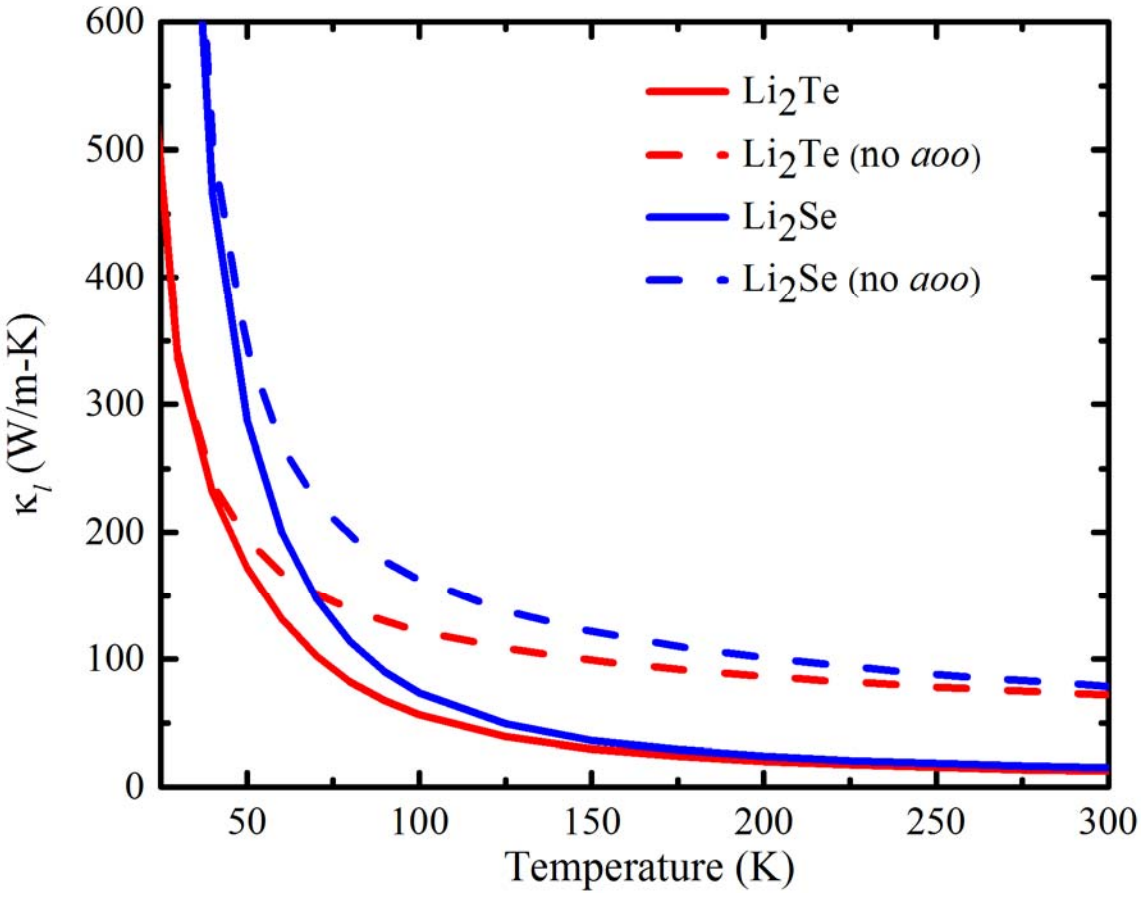

Figure 5: Comparison of calculated κ_l at low temperature with and without aoo scattering.

To further validate the important role of *aoo* scattering processes in limiting the otherwise possible high κ_l in these materials, we calculated κ_l of Li_2Te and Li_2Se while artificially eliminating contributions from *aoo* scatterings. We find that the isotopically pure room temperature κ_l increase significantly to 515 W/m-K and 583 W/m-K for Li_2Se and Li_2Te, respectively. These values are more in line with the expectations given by the six conditions outlined near the beginning of this article.

We also note that the strength of this scattering is frequency and temperature dependent. For temperatures well below the Debye temperature of a material the optic modes are not thermally excited, and will weaken *aoo* scattering. We find that *aoo* scattering is significant in Li_2Se and Li_2Te down to very low temperatures. It is only at significantly lower temperature (10-40K), where the optic modes are not thermally occupied, that the calculated κ values do not depend on *aoo* scattering processes that provide the dominant resistance at higher T. Figure 5 depicts this for Li_2Se and Li_2Te with naturally occurring isotope concentrations. Qualitatively similar curves can be produced for the isotopically pure cases though with much higher conductivities. This further underscores the importance of *aoo* scattering processes in determining κ_l for these systems. We note that at low temperature extrinsic scattering (*e.g.*, grain boundary scattering) can become significant.

It is informative to compare Li_2X systems with each other in regards to the conditions used to understand and estimate κ_l. Firstly, each system has the same number of phonon branches and similar average Grüneisen parameters $\bar{\gamma}$ (measure of anharmonicity) 1.21, 1.12, 1.11 and 1.08 for O, S, Se and Te, respectively. Thus κ_l is expected to be governed by θ_D, decreasing with increasing M_{avg} in going from O to S to Se to Te. This κ_l behavior is seen in the inset to Fig. 2, however, the decreasing behavior is slight when compared to the elemental series: diamond,

Si and Ge with calculated pure κ_l values of 3450 W/m-K, 155 W/m-K and 74 W/m-K, respectively. In going from diamond to Si, θ_D and bunching of acoustic branches decrease dramatically resulting in a 22 times reduction in κ_l due to increasing *aaa* scattering rates and lower acoustic velocities. Then going from Si to Ge the dispersions are qualitatively similar (no *a-o* gap, same acoustic bunching and optic bandwidth), thus the drop in κ_l is governed by reduced θ_D. In contrast, Li_2S, Li_2Se and Li_2Te have similar acoustic bunching so there are no dramatic κ_l differences. Further, as M_{avg} increases going from S to Se to Te, the *a-o* gap increases reducing *aao* scattering (increasing κ_l), while θ_D decreases (decreasing κ_l). These actions tend to balance out, and the importance of these changes in determining κ_l is masked by the dominant resistance provided by *aoo* scattering processes. Thus the variation of κ_l with mass is significantly less dramatic than that of the elemental, Boron-based and Beryllium-based compounds (inset to Fig. 2). Phonon-isotope scattering in the Li_2X systems is also of interest. We define the isotope effect, % enhancement to κ_l due to isotope purification, by $P = 100 \times (\kappa_{pure} / \kappa_{nat} - 1)$ where κ_{pure} and κ_{nat} are the κ_l values of isotopically pure and natural materials, respectively. The calculated room temperature P values for Li_2O, Li_2S, Li_2Se and Li_2Te are 6.52, 11.4, 17.7 and 18.8, respectively. These enhancements to κ_l are modest, and comparable to those of other low κ_l anti-fluorite structures Mg_2Si (P=11) and Mg_2Sn (P=4) [36]. More interestingly, however, are the changes that result to the phonon dispersions of Li_2X systems with isotope variation of the lighter Li atoms. Li has naturally occurring isotope abundances of ^{6}Li=7.6% and ^{7}Li=92.4%. Since the Li atoms are so light, varying the average Li mass through isotope modification significantly modulates the optic phonon branches: heavier mass decreases the frequencies, lighter mass increases the frequencies. In Li_2Se and Li_2Te the optic modes change little with pure ^{7}Li, but shift up in frequency by 6.5% for pure ^{6}Li. The

acoustic branches are not altered by this change in Li mass, thus the *a-o* gap increases significantly in these materials. There is no *aao* scattering in Li_2Te, however, for Li_2Se this leads to less intrinsic *aao* scattering, though κ_l is not much affected as the *aoo* scattering is the dominant resistance in this system.

IV. CONCLUSIONS

In summary, we investigated lattice thermal conductivities (κ_l) of Li_2X materials (X=O, S, Se, Te) using a linear phonon Boltzmann transport equation approach with *ab initio* force constants as input. Our calculations, both LDA and GGA, find low κ_l for these systems despite the presence of large *a-o* gaps and tightly bunched acoustic branches, conditions previously believed sufficient for high κ_l. Thus we find that the existing criteria for high κ_l are incomplete. Optic bandwidth and dispersive optic branches are also important considerations as they determine the phase space for *aoo* scattering, limiting the otherwise possible high κ_l for Li_2Se and Li_2Te here. The new criterion of optic bandwidth coupled with the six other conditions discussed previously presents a more informative and comprehensive understanding of κ_l behavior in materials, and provides an effective conduit for the discovery of new materials for both high and low κ_l applications.

Acknowledgements

S. M., L. L. and D. P. acknowledge support from the U. S. Department of Energy, Office of Science, Office of Basic Energy Sciences, Materials Sciences and Engineering Division and the National Energy Research Scientific Computing Center (NERSC), a DOE Office of Science

User Facility supported by the Office of Science of the U. S. Department of Energy under Contract No. DE-AC02-05CH11231. We thank Craig Bridges for many useful discussions.

* Corresponding author: lindsaylr@ornl.gov

APPENDIX A

Phonon dispersions:

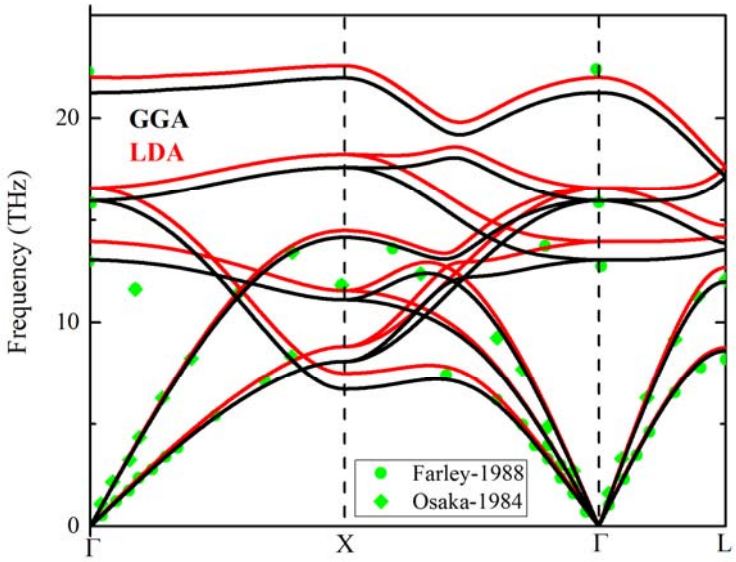

Figure 6: Phonon dispersions for Li_2O calculated with LDA (red) and GGA (black). Experimental data from Farley et. al. [53] and Osaka et. al. [54] are shown with green circles and diamonds, respectively.

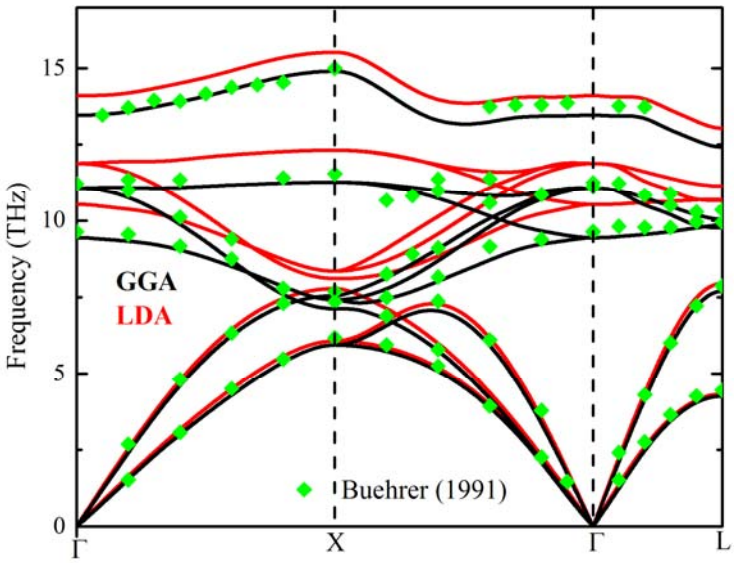

Figure 7: Phonon dispersions for Li_2S calculated with LDA (red) and GGA (black). Experimental data from Buehrer et. al. [55] are shown with green diamonds.

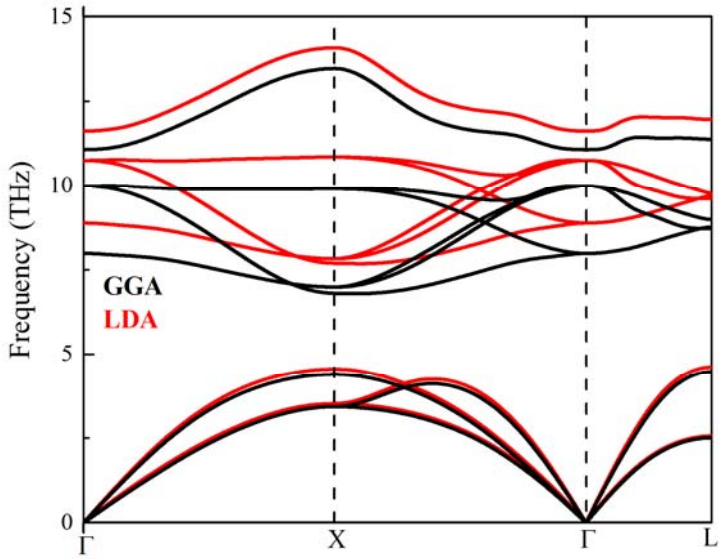

Figure 8: Phonon dispersions for Li_2Se calculated with LDA (red) and GGA (black).

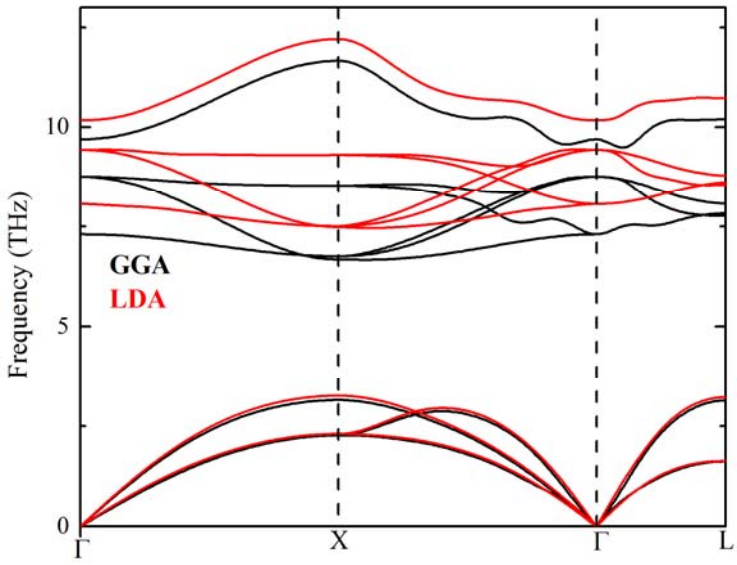

Figure 9: Phonon dispersions for Li_2Te calculated with LDA (red) and GGA (black).

APPENDIX B

Scattering Rates:

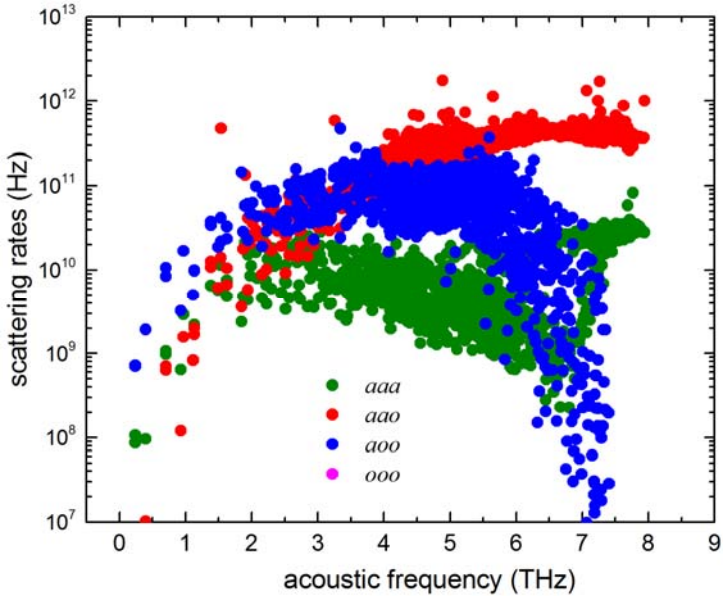

Figure 10: Calculated acoustic phonon scattering rates for aaa, aao, aoo and ooo processes in Li_2S.

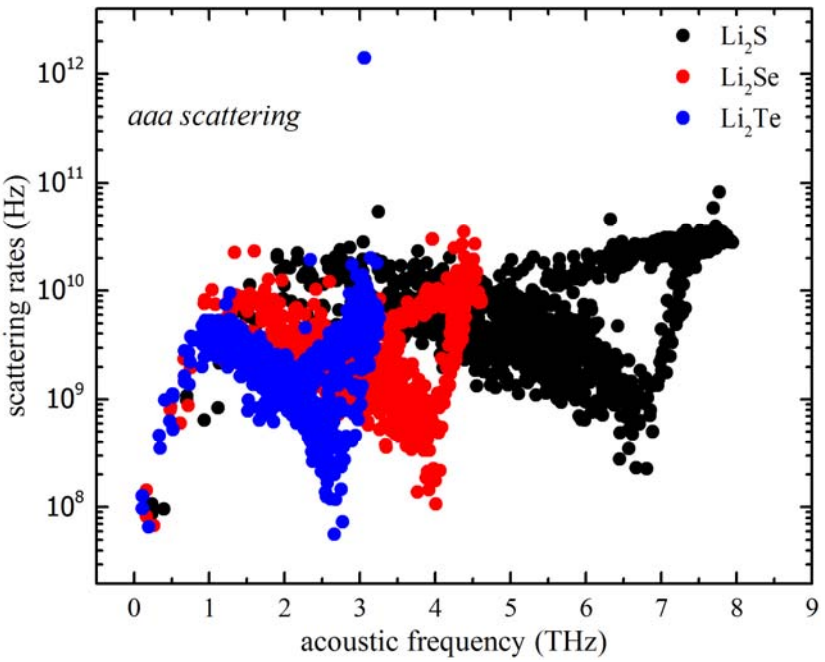

Figure 11: Comparison of calculated aaa scattering rates for Li_2S, Li_2Se and Li_2Te.

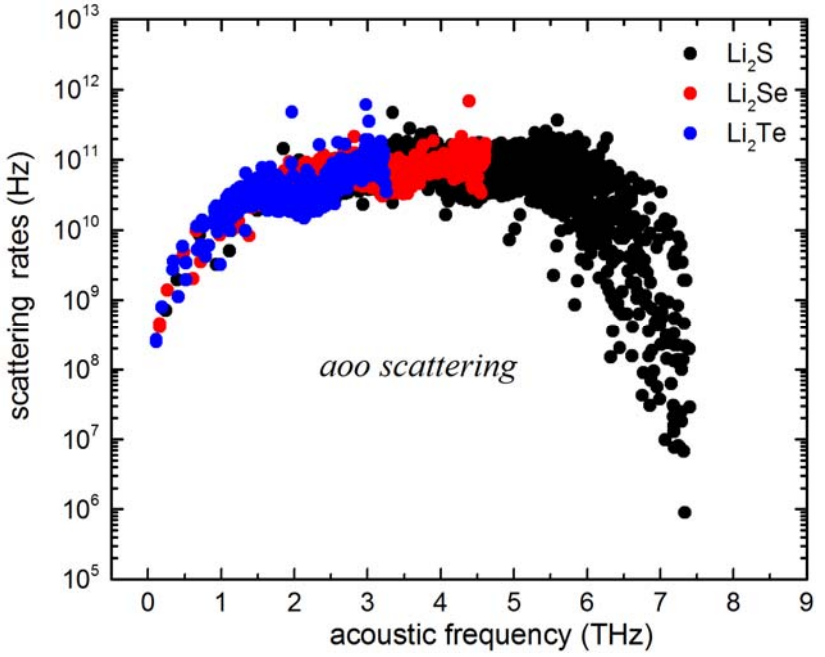

Figure 12: Comparison of calculated aoo scattering rates for Li_2S, Li_2Se and Li_2Te.

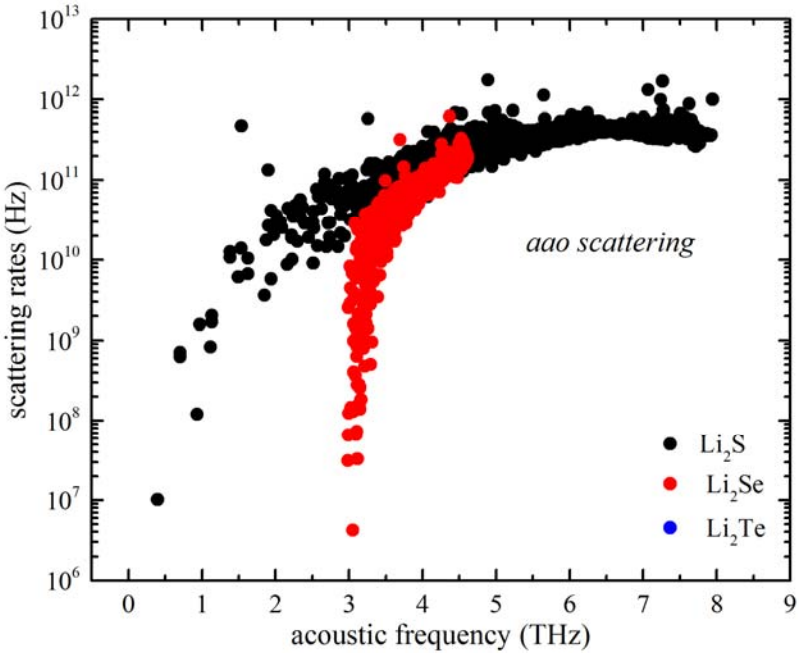

Figure 13: Comparison of calculated aao scattering rates for Li_2S, Li_2Se and Li_2Te.

References

[1] D. A. Broido, M. Malorny, G. Birner, N. Mingo, and D. A. Stewart, Appl. Phys. Lett. **91**, 231922 (2007).

[2] K. Esfarjani, G. Chen, and H. T. Stokes, Phys. Rev. B **84**, 085204 (2011).

[3] J. Garg, N. Bonini, B. Kozinsky, and N. Marzari, Phys. Rev. Lett. **106**, 045901 (2011).

[4] S. Mukhopadhyay and D. A. Stewart, Phys. Rev. Lett. **113**, 025901 (2014).

[5] X. L. Tang and J. J. Dong, Proc. Natl. Acad. Sci. USA **107**, 4539 (2010).

[6] F. Yang and C. Dames, Phys. Rev. B **87**, 035437 (2013).

[7] A. J. Minnich, J. A. Johnson, A. J. Schmidt, K. Esfarjani, M. S. Dresselhaus, K. A. Nelson, and G. Chen, Phys. Rev. Lett. **107**, 095901 (2011).

[8] Y. K. Koh and D. G. Cahill, Phys. Rev. B **76**, 075207 (2007).

[9] D. J. Singh and I. Terasaki, Nat. Mater. **7**, 616 (2008).

[10] P. Ball, Nature **492**, 174 (2012).

[11] A. Ward, D. A. Broido, D. A. Stewart, and G. Deinzer, Phys. Rev. B **80**, 125203 (2009).

[12] L. H. Wei, P. K. Kuo, R. L. Thomas, T. R. Anthony, and W. F. Banholzer, Phys. Rev. Lett. **70**, 3764 (1993).

[13] D. G. Onn, A. Witek, Y. Z. Qiu, T. R. Anthony, and W. F. Banholzer, Phys. Rev. Lett. **68**, 2806 (1992).

[14] A. A. Balandin, S. Ghosh, W. Z. Bao, I. Calizo, D. Teweldebrhan, F. Miao, and C. N. Lau, Nano Lett. **8**, 902 (2008).

[15] S. Ghosh, I. Calizo, D. Teweldebrhan, E. P. Pokatilov, D. L. Nika, A. A. Balandin, W. Bao, F. Miao, and C. N. Lau, Appl. Phys. Lett. **92**, 151911 (2008).

[16] G. A. Slack, J. Phys. Chem. Solids **34**, 321 (1973).

[17] D. T. Morelli, G. A. Slack, and *High Thermal Conductivity Materials* (SPRINGER, New York, 2005), p.^pp. 37.

[18] L. Lindsay, D. A. Broido, and T. L. Reinecke, Phys. Rev. Lett. **109**, 095901 (2012).

[19] L. Lindsay, D. A. Broido, and T. L. Reinecke, Phys. Rev. Lett. **111**, 025901 (2013).

[20] D. A. Broido, L. Lindsay, and T. L. Reinecke, Phys. Rev. B **88**, 214303 (2013).

[21] L. Lindsay, D. A. Broido, and T. L. Reinecke, Phys. Rev. B **88**, 144306 (2013).

[22] J. L. Ethridge, D. E. Baker, and A. D. Miller, J. Am. Ceram. Soc. **71**, C294 (1988).

[23] T. Takahashi and T. Kikuchi, J. Nucl. Mater. **91**, 93 (1980).

[24] J. U. Seo, G. K. Seong, and C. M. Park, Sci. Rep-Uk **5**, 7969 (2015).

[25] H. L. Shi, M. H. Du, and D. J. Singh, J. Alloy Compd. **647**, 906 (2015).

[26] P. Hohenberg and W. Kohn, Phys. Rev. B **136**, B864 (1964).

[27] W. Kohn and L. J. Sham, Phys. Rev. **140**, 1133 (1965).

[28] See Supplemental Material at URL for harmonic and anharmonic IFCs for Li_2X systems, LDA and GGA.

[29] http://www.quantum-espresso.org.

[30] R. D. Lide and R. P. H. Frederikse, *CRC Handbook of Chemistry and Physics* (Chemical Rubber Company Press, Boca Raton, FL, 1993), 74 edn.

[31] B. Bertheville, H. Bill, and H. Hagemann, J. Phys-Condens. Mat. **10**, 2155 (1998).

[32] Cunningh.Pt, S. A. Johnson, and E. J. Cairns, J. Electrochem Soc. **118**, 1941 (1971).

[33] E. H. Swanson, F. H. McMurdie, C. M. Morris, H. E. Evans, and B. Paretzkin, National Bureau of Standards Monograph 25 Section 10 Data for 84 Substances (1972).

[34] P. Haas, F. Tran, and P. Blaha, Phys. Rev. B **79**, 085104 (2009).

[35] P. Giannozzi *et al.*, J. Phys-Condens. Mat. **21** (2009).

[36] W. Li, L. Lindsay, D. A. Broido, D. A. Stewart, and N. Mingo, Phys. Rev. B **86**, 174307 (2012).

[37] L. Lindsay, D. A. Broido, and T. L. Reinecke, Phys. Rev. B **87**, 165201 (2013).

[38] N. Mingo, A. D. Stewart, A. D. Broido, L. Lindsay, and W. Li, in *Length-Scale Dependent Phonon Interactions*, edited by L. S. Shinde, and P. G. Srivastava (Springer, 2014).

[39] J. Fabian and P. B. Allen, Phys. Rev. Lett. **79**, 1885 (1997).

[40] M. K. Farr, J. G. Traylor, and S. K. Sinha, Phys. Rev. B **11**, 1587 (1975).

[41] A. E. Gheribi, A. Seifitokaldani, P. Wu, and P. Chartrand, J. Appl. Phys. **118**, 145101 (2015).

[42] A. Jain and A. J. H. McGaughey, J. Appl. Phys. **116**, 073503 (2014).

[43] M. Blackman, Philosophical Magazine **19**, 989 ((1935)).

[44] R. Cusco, J. Ibanez, N. Domenech-Amador, L. Artus, J. Zuniga-Perez, and V. Munoz-Sanjose, J. Appl. Phys. **107**, 063519 (2010).

[45] M. Kuball, J. M. Hayes, Y. Shi, and J. H. Edgar, Appl. Phys. Lett. **77**, 1958 (2000).

[46] J. W. Pomeroy, M. Kuball, H. Lu, W. J. Schaff, X. Wang, and A. Yoshikawa, Appl. Phys. Lett. **86**, 223501 (2005).

[47] G. P. Srivastava, J. Phys-Condens. Mat. **21**, 174205 (2009).

[48] S. P. Hepplestone and G. P. Srivastava, Phys. Rev. B **74**, 165420 (2006).

[49] L. Lindsay, D. A. Broido, and N. Mingo, Phys. Rev. B **80**, 125407 (2009).

[50] T. Shiga, J. Shiomi, J. Ma, O. Delaire, T. Radzynski, A. Lusakowski, K. Esfarjani, and G. Chen, Phys. Rev. B **85**, 155203 (2012).

[51] J. Al-Otaibi and G. P. Srivastava, J. Phys-Condens. Mat. **27**, 335801 (2015).

[52] S. Lee, K. Esfarjani, T. F. Luo, J. W. Zhou, Z. T. Tian, and G. Chen, Nat. Commun. **5**, 3525 (2014).

[53] T. W. D. Farley, W. Hayes, S. Hull, R. Ward, M. T. Hutchings, and M. Alba, Solid State Ionics **28**, 189 (1988).

[54] T. Osaka and I. Shindo, Solid State Communications **51**, 421 (1984).

[55] W. Buehrer, F. Altorfer, J. Mesot, H. Bill, P. Carron, and H. G. Smith, J. Phys-Condens. Mat. **3**, 1055 (1991).